Ecosystem fluxes of carbonyl sulfide in an old-growth forest: temporal dynamics and responses to diffuse radiation and heat waves

Bharat Rastogi[1], Max Berkelhammer[2], Sonia Wharton[3], Mary E Whelan[4] Frederick C. Meinzer[5], David Noone[6], and Christopher J. Still[1]

[1] Department of Forest Ecosystems and Society, Oregon State University, OR 97331, USA
[2] Department of Earth and Environmental Sciences, University of Illinois at Chicago, Chicago, Illinois, USA
[3] Atmospheric, Earth and Energy Division, Lawrence Livermore National Laboratory, 7000 East Avenue, L-103, Livermore, CA 94550, USA
[4] Carnegie Institution for Science, 260 Panama St., Stanford, CA, USA, 94305

[5] USDA Forest Service, PNW Research Station, Corvallis, OR 97331, USA

[6] College of Earth, Ocean and Atmospheric Sciences, Oregon State University, OR 97331, USA

Corresponding author: Bharat Rastogi (bharat.rastogi@oregonstate.edu)

Abstract

Carbonyl sulfide (OCS) has recently emerged as a tracer for terrestrial carbon uptake. While physiological studies relating OCS fluxes to leaf stomatal dynamics have been established at leaf and branch scales and incorporated in global carbon cycle models, the quantity of data from ecosystem-scale field studies remains limited. In this study, we employ established theoretical relationships to infer ecosystem-scale plant OCS uptake from mixing ratio measurements. OCS fluxes showed a pronounced diurnal cycle, with maximum uptake during mid-day. OCS uptake was found to scale with independent measurements of CO_2 fluxes over a 60-m-tall old-growth forest in the Pacific Northwestern U.S. (45°49′13.76″ N; 121°57′06.88″) at daily and monthly timescales under mid-high light conditions across the growing season in 2015. OCS fluxes tracked changes in soil moisture, and were strongly influenced by the fraction of downwelling diffuse light. Finally, we examine the effect of sequential heatwaves on fluxes of OCS, CO_2 and H_2O. Our results bolster previous evidence that ecosystem OCS uptake is strongly related to stomatal dynamics, and measuring this gas improves constraints on estimating photosynthetic rates at the ecosystem scale.

1. Introduction

Carbonyl Sulfide (OCS) is the most abundant sulfur gas in the atmosphere, with a mean atmospheric concentration of ~500 ppt (parts per trillion), and therefore a significant part of the tropospheric and stratospheric sulfur cycles, with implications for the global radiation budget and ozone depletion (Johnson et al.,1993; Notholt et al., 2003). The dominant sink of atmospheric OCS is vegetation (Kesselmeier and Merk, 1993; Kettle et al., 2002; Montzka et al., 2007 and references therein), through rapid and irreversible hydrolysis by the ubiquitous enzyme carbonic anhydrase (Protoschill-Krebs, Wilhelm, &

43 Kesselmeier, 1996; Protoschill-Krebs and Kesselmeier, 1992). Recent advances in
44 spectroscopic technology have enabled continuous in-situ measurements of OCS on
45 timescales that are relevant to understanding stomatal function at the leaf-scale (Stimler
46 et al., 2010a, 2010b), branch scale (Berkelhammer et al., 2014) and the ecosystem scale
47 (Kooijmans et al., 2017; Wehr et al., 2017). An important distinction between OCS and
48 CO_2 cycling is the absence of a retroflux from actively photosynthesizing leaves (OCS
49 emissions have been reported from stressed crops following severe fungal infection;
50 Bloem et al., 2012). However, the normalized leaf uptake ratio of OCS:CO_2 (LRU;
51 Sandoval-Soto et al., 2005) is relatively constant at medium to high light levels (Maseyk
52 et al., 2014; Stimler et al., 2010), making it an excellent proxy for quantifying plant
53 productivity (GPP; Asaf et al., 2013; Billesbach et al., 2014; Blonquist et al., 2011). On
54 the other hand, both uptake and emissions of OCS from soils have been identified
55 (Whelan et al., 2016; Sun et al., 2015; Maseyk et al., 2014; Kesselmier et al., 1999).
56 While ecosystem-scale measurements of OCS continue to establish links between OCS
57 uptake and GPP in different ecosystems (for a comprehensive list of ecosystem scale
58 studies readers are referred to Figure 2 in Whelan et al., 2017), inconsistencies persist.
59 For example, in an oak-savanna woodland in southern France Belviso et al. (2016) found
60 that OCS exchange was strongly influenced by photosynthesis during early morning
61 hours, while meaningful values of LRU could only by calculated for a few days in the
62 early afternoons. Commane et al. (2015) were unable to explain mid-summer emissions
63 of OCS at a mid-latitude deciduous forest. Uncertainties highlighted above argue for
64 field-scale measurements of OCS in a variety of ecosystems, particularly as OCS flux
65 predictions have recently been incorporated to inform estimates of plant productivity in
66 global carbon cycle models (Campbell et al., 2017a; Hilton et al., 2017; Launois et al.,
67 2015).
68
69 OCS fluxes have not been previously reported for old-growth forests, although a recent
70 study using flask samples inferred large uptake of OCS in coastal redwood forests in
71 northern California (Campbell et al., 2017b). Rastogi et al. (in revision) found large
72 drawdowns in mixing ratios of OCS at an old growth forest in the pacific northwestern
73 U.S., and significant uptake of this gas by various components of the ecosystem (leaves,
74 soils, and epiphytes). In this study, we report estimates of OCS fluxes from an old-growth
75 forest and place them in the context of ecosystem carbon and water cycling. Additionally,
76 we investigate the response of CO_2, H_2O and OCS fluxes to changes in the fraction of
77 downwelling diffuse radiation, as well as heat wave events through the growing season.
78 Technological constraints posed limitations in measuring fast-response OCS fluxes so
79 instead we combine continuous in-situ measurements of OCS mixing ratios above and
80 within the canopy with established theoretical equations for OCS uptake (see Berry et al.,
81 2013; Commane et al., 2015; Seibt et al., 2010) to characterize OCS fluxes using a simple
82 empirical model and compare them with ecosystem uptake of CO_2 from co-located eddy
83 covariance measurements.
84
85 **2. Methods**
86 2.1. Site Description
87 Measurements were made at the Wind River Experimental Forest (WR), located within
88 the Gifford Pinchot National Forest in southwest Washington state, USA (45°49′13.76″

89　N; 121°57′06.88″; 371 m above sea level). The site is well studied and described in great
90　detail (Paw U et al., 2004; Shaw et al., 2004; Wharton and Falk, 2016; Winner et al.,
91　2004). The climate is classified as temperate oceanic with a strong summer drought. The
92　forest is 478 ha of preserved old-growth evergreen needle-leaf forest, with dominant tree
93　species of Douglas fir (*Pseudotsuga menziesii*) and Western hemlock (*Tsuga*
94　*heterophylla*). The tallest Douglas fir trees are between 50 and 60m, while the shade-
95　tolerant hemlocks are typically between 20-30 m high. Maximum rooting depth is 1–2 m
96　for the tallest, dominant Douglas-fir trees although most of the root biomass is
97　concentrated in the first 0.5 m (Shaw et al., 2014). The cumulative LAI is estimated to be
98　8-9 $m^2 m^{-2}$ (Parker et al., 2004). Additionally, the ecosystem hosts a large diversity of
99　mosses, lichens and other epiphytic plants, which play an important role in canopy OCS
100　dynamics (Rastogi et al., in revision). The soils are volcanic in origin, although most of
101　the forest surface is comprised of decaying organic matter (Shaw et al., 2004).
102
103　2.2. Study period: Measurements reported here are between April 18- Dec 31, 2015.
104　However, in early November an intake line at the top of the canopy was damaged after a
105　rainstorm. Measurements continued at the other intake heights (see sections 2.4 and 2.9).
106　Therefore, ecosystem fluxes and related analyses in this study cover 136 days between
107　April 18 and October 31, while chamber based soil fluxes are reported for the months of
108　August-December. Gaps in the time series due to analyzer maintenance correspond to Jun
109　26-28, July 6-17, August 4-7, August 24 and October 4-7. April-October roughly
110　corresponds to most of the growing season, although at this site GPP usually peaks early
111　in March-April, when soil moisture is high and ecosystem respiration flux is low, while
112　plant productivity is typically severely light and temperature limited in the months of
113　November-December (Wharton and Falk, 2016). Environmental conditions during the
114　measurement campaign are shown in Figure 1 are represent a typical Mediterranean-type
115　climate, with temperature peaking in July and minimal to no measured rainfall between
116　June and September. This results in high summertime atmospheric vapor pressure deficit
117　(VPDa), and soil moisture declines steadily through the summer period, with some
118　recharge following rare precipitation events in September and then more commonly in
119　October. The measurement period also encompasses three distinct heat waves,
120　characterized by anomalously high air temperatures and mid-day VPDa values (often
121　exceeding 4 kPa). We examine the response of OCS and CO_2 fluxes during these heat
122　waves.
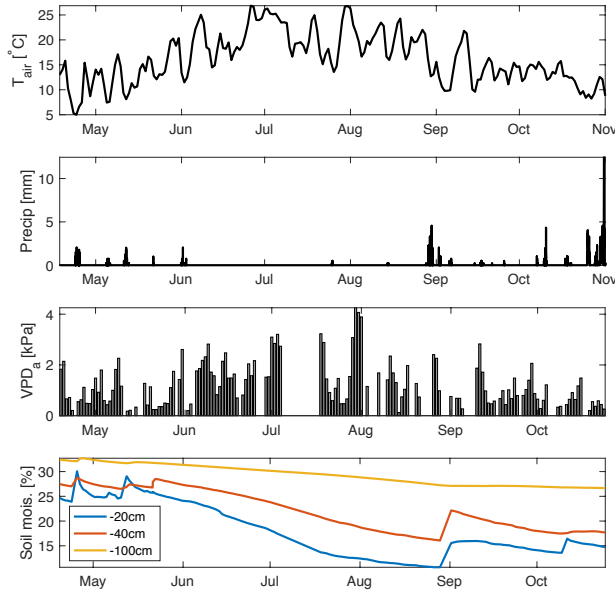
Figure 1. Environmental conditions at Wind River during the measurement campaign.
daily mean air temperature (a), precipitation (b) mid-day VPDa (c) and soil moisture
measured at three depths (d) are shown.

2.3. CO_2 and H_2O eddy flux measurements: Carbon, water and energy fluxes have been
collected since 1998 at the Wind River AmeriFlux tower (US-wrc; Paw U et al. 2004).
For further details readers are referred to Falk et al., (2008; instrumentation and data
processing), and Wharton et al., (2012) and Wharton and Falk, (2016) for multi-year
carbon and water flux measurements and synthesis.

2.4. OCS measurements: A commercially available off-axis integrated cavity output
spectroscopy analyzer manufactured by Los Gatos Research Inc., (LGR; model 914-
0028) was deployed at the base of the tower in an insulated and temperature-controlled
shed. The instrument measures mixing ratios of OCS, CO_2, H_2O and CO simultaneously
at a maximal scan rate of 5Hz. The system uses a 4.87 µm cascade laser coupled to a high
finesse 800 cm^3 optical cavity and light transmitted through the cavity is focused into a
cooled and amplified HgCdTe detector. OCS is detected at ~2050.40 cm^{-1}, CO_2 at
2050.56 cm^{-1}, CO at ~2050.86 cm^{-1}, and H_2O at ~2050.66 cm^{-1}. Pressure broadening
associated with changes in the concentration of water vapor in the samples is corrected
for in the analysis routine. Air was sampled through 0.25'' diameter PFA tubing using a
diaphragm pump at a flow rate of 2L min^{-1}, from inlets located at 70m (at the height of
the eddy flux instrumentation), 60m (canopy top), 20m, 10m, and 1m. The sampling
frequency was 0.1Hz and the sampling interval was 5 minutes. The first minute of each
sampling interval was removed to avoid any inter-sampling mixing. The remaining data
were checked for temperature and pressure fluctuations inside the measurement chamber,
and a moving window filter was used to eliminate any sudden outliers in the data. Mixing
ratios were aggregated to provide hourly means. For detailed information regarding
instrumentation and the measurement readers are referred to Rastogi et al (in revision),
Berkelhammer et al. (2014) and Belviso et al. (2016).

152   2.5. Calibration: Calibration was performed using ambient air stored in insulated tanks as
153   a secondary reference. Air was sampled into the analyzer daily, and tank pressure was
154   routinely monitored to check for leaks. Glass flasks were randomly sampled from
155   calibration tanks and measured against a NOAA GMD reference standard. Cross-
156   referencing revealed that the accuracy of the measurement was within the reported
157   minimum uncertainty of the instrument (of 12.6 pmol mol^{-1}; Berkelhammer et al., 2016).
158

159   2.6. Thermal Camera measurements: Leaf temperatures were measured from October 28,
160   2014 to January 28, 2016 using a FLIR A325sc thermal camera (FLIR System Inc.,
161   Wilsonville, OR), in which a FLIR IR 30-mm lens (focal length: 30.38 mm; field of
162   view: 15°×11.25°) was installed. The thermal camera has a pixel resolution of 320×240.
163   Within the field of view (FOV), spot sizes of a single pixel are 0.83 cm from 10-m
164   distance and 8.3 cm from 100-m distance. Manufacturer-reported errors in original
165   measured thermal temperatures are ±2 °C or ±2% of the measurements. The camera
166   model is identical to one used in another study at an AmeriFlux site in central Oregon
167   (US Me-2), and the detailed specifications can be found in Kim et al. (2016). To monitor
168   a larger canopy region, a pan-tilt unit (PTU) was used for motion control, allowing
169   multiple canopy thermal image acquisition within one motion cycle. We used a FLIR
170   PTU-D100E (FLIR System Inc., Wilsonville, OR; (http://www.flir.com/mcs) to move the
171   thermal camera vertically and horizontally at specific pan and tilt angles. We selected
172   five pan-tilt angle (PT) positions representing the upper canopy (i.e., ~40 to 60 m above
173   the forest floor) to estimate leaf temperatures in this study.

174   2.7. Diffuse light measurement and analyses: An SPN1 Sunshine Pyranometer (Delta-T
175   Devices ltd., Cambridge, U.K.) was installed at the top of the canopy and collected direct
176   and diffuse shortwave downwelling radiation from April- December 2015. Measurements
177   were made every 1 min, and then aggregated to hourly means. We limited our analyses of
178   diffuse radiation data to include only mid-day hours (between 11am-1pm) to minimize
179   the influence of solar angles on diffuse radiation fractions. We defined three distinct
180   periods based on the ratio of diffuse radiation to total incoming solar radiation (*fidff*).
181   Data were characterized as clear if *fdiff* < 0.2; partly cloudy if *fdiff* > 0.2 and *fdiff* < 0.8,
182   and overcast if *fdiff* > 0.8.

183   2.8. OCS flux estimation: 'Canopy-scale leaf' OCS flux was estimated using flux-
184   gradient similarity, following Commane et al., 2015.

$$F_{OCS} = F_{H2O} \cdot \frac{g_{OCS}}{g_{H2O}} \tag{1}$$

186

187   where F_{OCS}, F_{H2O}, g_{OCS} and g_{H2O} are the fluxes and gradients of OCS and H_2O,
188   respectively. Following Seibt et al., (2010) and Berry et al., (2013), we assume that OCS
189   is irreversibly and rapidly consumed inside leaves, such that the gradient between
190   ambient air and the leaf interior effectively reduces to the ambient measured OCS mixing
191   ratio:

192

$$g_{OCS} = \chi^a_{OCS} - \chi^l_{OCS} = \chi^a_{OCS} \quad , \tag{2}$$

194   where g_{OCS} is defined as he gradient of OCS between ambient air and the leaf
195   intercellular spaces (χ is the mixing ratio of OCS and superscripts *a* and *l* refer to ambient

196 and leaf respectively). In our study, χ^a_{OCS} is the measured mixing ratio at the canopy top
197 (60m) instead of above canopy (70m) to account for turbulent transport between the
198 canopy top and air that is above the canopy top. We use vapor pressure deficit (VPD) as
199 the corresponding gradient for H_2O, under the key assumption that the intercellular leaf
200 surfaces are saturated with water vapor. While VPD is usually calculated using air
201 temperature, a more accurate calculation can be performed with leaf temperatures, which
202 can deviate significantly from air temperatures (Kim et al. 2016), leading to significant
203 differences between the VPD of ambient air and that at the leaf surface (Fig. 2a and 3d in
204 this study). Previously leaf temperatures have been inferred from sensible heat fluxes,
205 wind speed and air temperatures (e.g. Wehr et al., 2017), here we use explicit
206 measurements of leaf skin temperatures to estimate leaf-air VPD (VPD_l). Analogous to
207 Eq (3),
208

$$g_{H2O} = \chi^l_{H2O} - \chi^a_{H2O} = \frac{(e_i - e_a)}{P} = \frac{VPD_l}{P} \quad , \tag{3}$$

210 where e_i is saturation vapor pressure in the leaf sub-stomatal cavity (kPa), using leaf skin
211 temperature, ea is the actual vapor pressure (kPa), P is the measured atmospheric pressure
212 (kPa) at the tower top, and $\chi^l_{H_2O}$ and $\chi^a_{H_2O}$ (ppth) are the leaf and ambient H_2O mixing
213 ratios at the canopy top. Finally, since gradients of OCS and H_2O are estimated between
214 ambient air and the leaf intercellular spaces, these are normalized by the ratio of
215 diffusivities of these two species in air (Seibt et al., 2010; Wohlfahrt et al., 2012).
216

217 F_{H2O} was measured using eddy covariance at the tower top (70m). In high LAI forests
218 with minimal exposed soil, such as those of the Pacific Northwest, fluxes of F_{H2O} can be
219 treated as a good proxy for transpiration, since soil evaporation should be minimal. We
220 excluded rainy days, as well as two days following rainfall, to only capture periods when
221 F_{H2O} can be assumed to be dominated by transpiration. Equation (1) was evaluated only
222 under the condition $F_{H2O} > 0.2$ mmolm^{-2}s^{-1}. We restricted our analyses to daytime, when
223 OCS flux is assumed to be related to leaf CO_2 uptake (Maseyk et al., 2014; Wehr et al.,
224 2017).
225

226 Leaf Relative uptake was calculated following Seibt et al (2010).
227

$$LRU = \frac{F_{OCS}}{GPP} \cdot \frac{\chi CO_2}{\chi OCS} \quad , \tag{5}$$

229

230 where GPP was estimated from CO_2 fluxes measured at the tower top, using a nighttime
231 based partitioning approach (Reichstein et al., 2005), that was optimized for the site (Falk
232 et al., 2008). Finally, canopy conductance (Gc) was estimated using a simple flux-
233 gradient approach with the assumption that the canopy (or ecosystem) acts as a single big
234 leaf.

$$Gc = F_{H2O} \cdot \frac{VPD_l}{P} \quad , \tag{6}$$

236

237 2.9. Surface Fluxes: A long-term automatic soil survey chamber (Li-Cor 8100-104, 20
238 cm diameter) was installed at three 0.03 m^2 surface sites in series, within 1 meter of each
239 other. All plastic and rubber parts had been removed from the chamber and replaced with
240 materials compatible with OCS measurements: stainless steel, PFA plastic, and Volara

241 foam. Blank measurements were performed in the laboratory before deployment and
242 OCS concentrations in the chamber were found to be statistically indistinguishable from
243 incoming ambient concentrations. The stainless-steel chamber top opened and closed
244 automatically on a timer. Gas was drawn through the chamber via a pump downstream of
245 the analyzer, and the 3 Lmin[-1] flow rate was confirmed with a mass flow meter. When the
246 chamber was open, ambient near-surface air was observed. When the chamber was
247 closed, trace gas concentrations reached a stable state for at least 2 minutes during the 10-
248 minute incubation time. The difference between the ambient concentration and the stable
249 closed-chamber concentration were used to calculate the surface fluxes of OCS and CO_2.

$$F_{forest\,floor} = M_c \Delta\chi . A^{-1} \, , \tag{7}$$

251 where M_c is the measured flow rate into the chamber (converted from Lmin[-1] to mols[-1]
252 using the ideal gas law) and $\Delta\chi$ is the difference between mixing ratios of OCS or CO_2 in
253 ambient air and the chamber and A is the surface area of the chamber. The minimum flux
254 detectable with this method was 1.2 pmolm[-2]s[-1] uptake or production.

255 Care was taken to select sites characteristic of the surface, which was generally springy
256 and covered in a mat of mosses and lichen. Surface flux observations were made at site 1
257 from July 6 to 16, site 2 from August 13 to October 7, and site 3 from November 6 to
258 December 2, 2015. The first site was visually similar to the subsequent two sites at the
259 surface, though the chamber base of the first site was installed into the moss layer and a
260 barely decomposed fallen tree. When a soil sample was attempted to be extracted from
261 the footprint of the chamber base, several liters of intact wood litter were removed. The
262 influence of the developed soil on site 1 is therefore considered minimal. Site 2 was
263 selected nearby and observations were made until a dominant tree fell on the soil
264 chamber. The chamber was repaired and re-installed a month later at site 3 and
265 observations continued without incident until the chamber was removed in advance of the
266 soil freezing.

3. Results and Discussion:

268 3.1. Ecosystem fluxes: The composite diurnal cycles for CO_2, water vapor and OCS and
269 fluxes are shown (Fig. 2a-c). The total ecosystem flux of OCS (F_{OCS}; Fig 2.b.) follows a
270 pronounced diurnal cycle that peaks during daylight hours. The vertical profile of mixing
271 ratios measured throughout the canopy is also shown (right y-axis and orange lines in
272 Fig.2.b). OCS mixing ratios are highest at the canopy top and lowest near the forest floor,
273 but mixing ratios increase from the early morning to mid-afternoon. Together these
274 processes are indicative of ecosystem uptake and downward entrainment of boundary
275 layer air. While entrainment helps explain the diurnal cycle of observed mixing ratios,
276 this flux integrates to zero at daily and longer time scales (Rastogi et al., in revision). The
277 shape of the F_{OCS} curve is very similar to those of net and gross carbon fluxes (Fig 2.b-c),
278 although F_{OCS} was consistently negative throughout the 24-hour period, implying
279 ecosystem uptake during nighttime and daylight hours. While nighttime uptake of OCS
280 (mean nighttime flux $\sim$ -10 $\pm$ 1 pmolm[2]s[-1]) is likely due to a combination of soil,
281 epiphyte, and vascular plant uptake due from partially closed stomata, daytime uptake is
282 likely dominated by vascular plant stomatal activity. Leaf relative uptake, a ratio of
283 F_{OCS}:GPP normalized by the mean mixing ratios of OCS:CO_2, showed a strong light

284 dependence. High-light, mid-day values ranged between 3-4, which is higher than those
285 observed at other forest systems (Kooijmans et al., 2017; Wehr et al., 2017) but well
286 within the spread of values obtained in a recent meta-analyses of OCS studies for
287 vegetated ecosystems (Whelan et al., 2018). The diurnal cycle was found to be
288 asymmetric, with peak values observed in the early morning, when stomatal conductance
289 is likely to be high (Winner et al., 2004), but GPP is limited by low light levels. It is
290 important to note that LRU is likely influenced by large amounts of epiphyte and
291 understory vegetation, which assimilate OCS even at times when ecosystem CO_2 uptake
292 is low or zero. Epiphytic assimilation of OCS is highly influenced by moisture content
293 (Gimeno et al., 2017) and is typically higher through the night and in the early mornings
294 at this site (Rastogi et al., in revision). Moreover, in tall old-growth forests, leaf area is
295 vertically distributed over a much larger part of the canopy compared to other forests
296 (Parker et al., 2004). While leaves at the canopy top exercise tight stomatal control to
297 limit water loss and minimize hydraulic failure (Woodruff et al., 2007) leaves lower
298 down in the canopy, including those of understory vegetation, likely impose less stomatal
299 control of transpiration (Winner et al., 2004). Lower-canopy leaves may therefore
300 continue to disproportionately assimilate OCS, even under low rates of carbon
301 assimilation (as CO_2 uptake is additionally light limited).
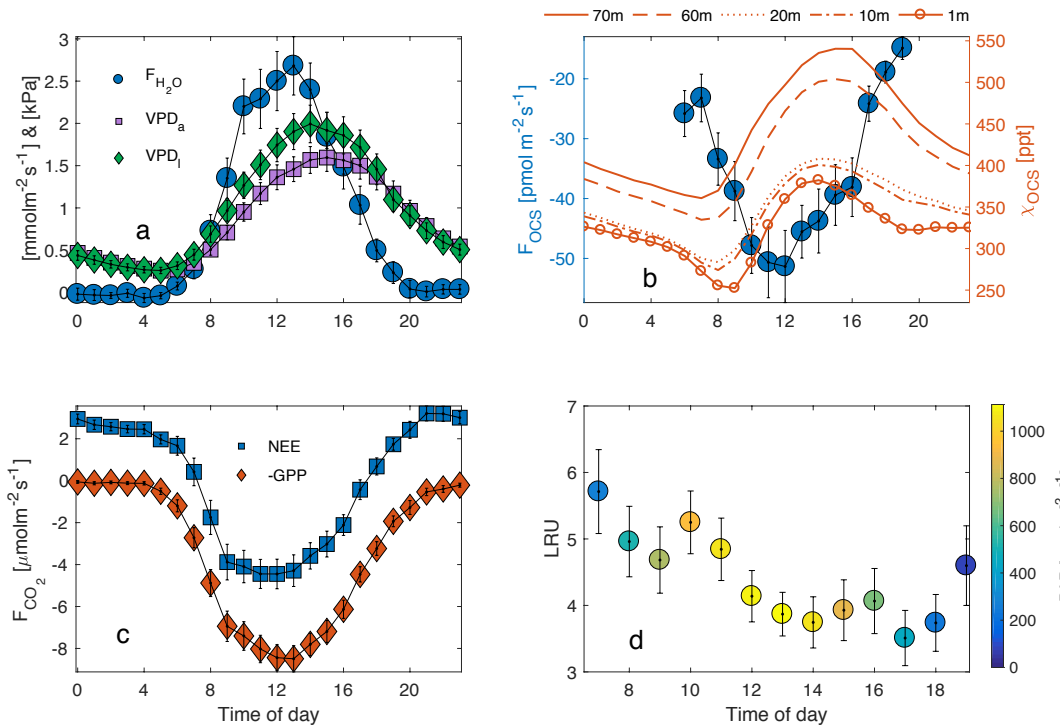
303 Figure 2. Diurnal cycle of H_2O flux (blue circles) and VPD estimated from air and leaf
304 temperatures (purple squares and green diamonds respectively; a), estimated OCS flux
305 (circles, left axis) and mixing ratio profile (right axis; b), NEE and GPP (blue squares and
306 red diamonds; c), and leaf relative uptake (calculated only during daylight hours, colors
307 represent Photosynthetically active radiation; d). Vertical bars indicate standard error.

309 3.2. Daily and seasonal dynamics: Daytime fluxes of OCS were correlated to independent
310 estimates of GPP (Fig. 3a), and uptake of both OCS and CO_2 reduced as soil moisture
311 declined. Variability in the relationship between fluxes of OCS and CO_2 and soil
312 moisture was related to VPD, which fluctuated as a response of changing cloud cover
313 (discussed later in sec. 3.4).
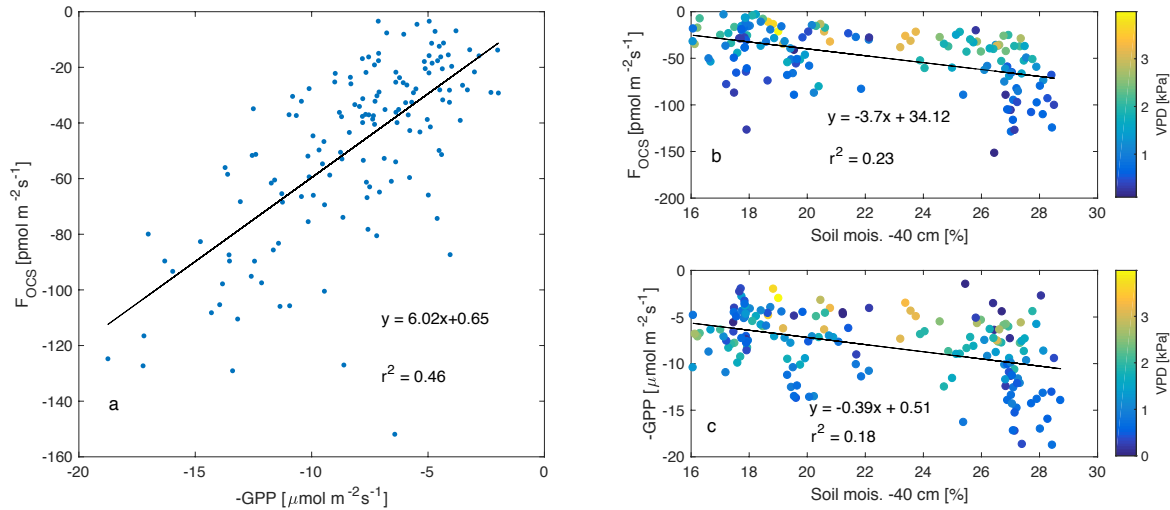
314

315 Figure 3. F_{OCS} was linearly correlated to GPP (plotted as a negative quantity to show
316 ecosystem uptake; a), while both FOCS and GPP reduced as a function of decreasing soil
317 moisture (b-c). Data presented here are mid-day means, data in (b-c) are colored
318 according to VPD.

319   Ecosystem uptake of OCS and CO_2 (as well as GPP) was highest in April (Fig. 4a), and
320 declined as the soil drought progressed (Fig. 4f). Mean monthly maximum OCS flux was
321 estimated as -61 ± 6 pmolm^{-2}s^{-1}, while daily mean maximum GPP over this period was
322 estimated as $10 \pm 1\mu$molm^{-2}s^{-1} (plotted as a negative quantity in Fig. 4b to show
323 ecosystem uptake). While the steepest declines in F_{OCS}, NEE and GPP happened between
324 the months of May and June, F_{OCS} continued to decline through the rest of the summer,
325 with a minimum in August, and remaining low in September and October. CO_2 fluxes
326 flattened between June-September, before declining again in October. While uptake of
327 OCS and CO2 followed similar patterns, H_2O flux remained high until mid-summer (Fig.
328 4c) before plunging in August, presumably due to a combination of high VPD (Fig. 4d)
329 and declining soil moisture (Fig. 4f), as plants exercised greater control over stomata.
330 This can be clearly seen in the seasonal cycle of canopy conductance (Gc; Fig. 4e). Mean
331 monthly Gc was highest in the months of April and May, and then declined in response to
332 increasing VPD and decreasing soil moisture, before increasing again slightly in
333 September and October following soil recharge and decreased VPD due to precipitation
334 events. In October, soil water recharge, several rain-free days (Fig. 1), and lower VPD
335 (Fig. 4d) do not result in increased gas exchange, likely due to downregulation of
336 photosynthesis (Eastman and Camm, 1995), induced by photoprotective changes in the
337 xanthophyll cycle (Adams and Demmig-Adams, 1994).
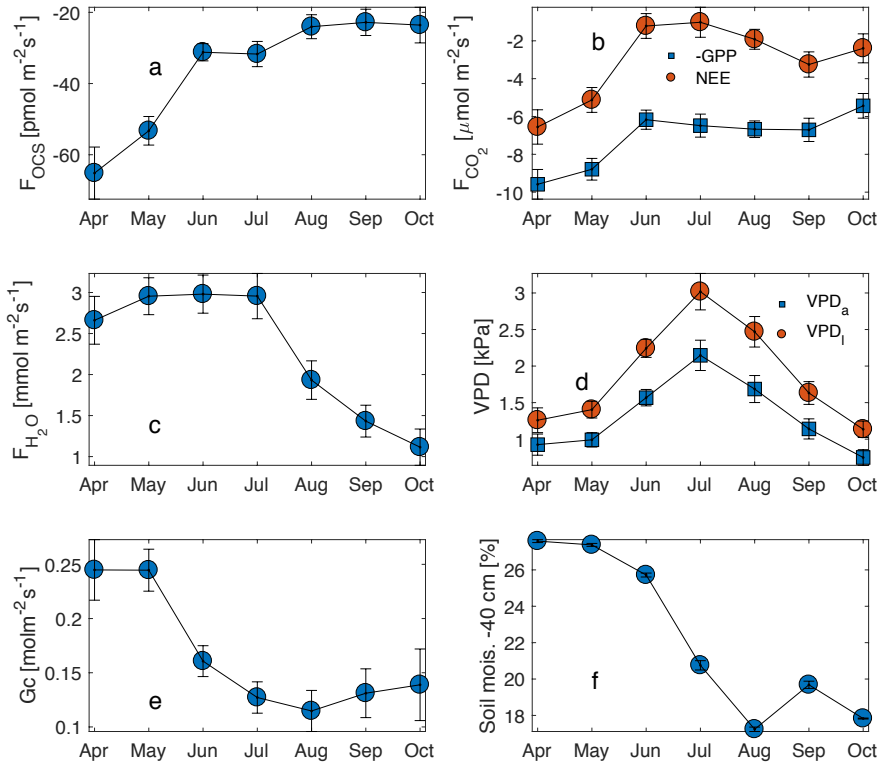
9

Figure 4. Monthly means for daytime F_{OCS}, NEE and -GPP (red circles and blue squares; b), water vapor flux (c), VPD_a and VPD_l (blue squares and red circles; d), canopy conductance (Gc; e), and soil moisture at -40cm depth (f). Vertical bars indicate standard error.

3.3. Surface Fluxes: Forest floor OCS fluxes were observed from 3 sites in series and within 1 m of each other. Site 1 had approximately twice the OCS uptake compared to the subsequent two sites and had a substantial layer of intact woody debris under the chamber footprint. Site 2 and 3 had OCS fluxes similar to previous surface fluxes reported for forests (Whelan et al., 2018). For all sites, there was no clear diurnal pattern. For site 2, uptake immediately following chamber installation was higher (~6 pmol m^{-2}s^{-1}) than fluxes later on (all <6 pmol m^{-2}s^{-1}) when temperatures were lower (Fig 5). Site 3 did not have high uptake after chamber installation, and had consistent fluxes between the detection limit and -6.2 pmol m^{-2}s^{-1} for the first few weeks. When ambient air temperatures dropped below freezing, uptake remained unchanged, except for the largest uptake observed (6 to 12 pmol m^{-2}s^{-1}) during two events when average air temperature fluctuated from a cooling to warming trend. Soil temperature never dropped below freezing during the experiment and was generally colder over time. We did not observe any OCS emissions from the chamber based measurements, consistent with recent studies that find that cooler, moist (Maseyk et al., 2014; Sun et al., 2016; Whelan et al., 2016) and radiation limited (Kitz et al., 2017) soils do not emit OCS.

Surface CO$_2$ emissions exhibited a relationship with temperature, where highest production (~25 μmol m^{-2}s^{-1}) corresponded with temperatures ~15°C, and maximum flux values decreased for warmer and colder temperatures. CO$_2$ emissions had a diurnal

362 pattern, with lowest emissions at night and maximum emissions in late morning to mid-
363 afternoon. No obvious relationship emerges from CO_2 emission and OCS uptake, though
364 the high OCS uptake events in late November and early December have a linear
365 relationship with CO_2 emissions. For sites 2 and 3, the ratio of OCS emission to CO_2
366 production, normalized by the concentration of OCS and CO_2 in the closed chamber, was
367 between -0.25 and -3.5 with a mean of -1. In contrast, the same ratio for site 1 varied
368 from -5 to -19 with a mean of -10.

369
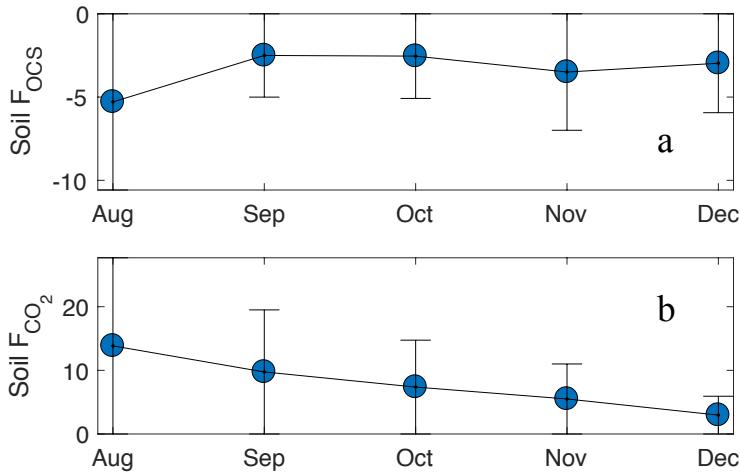
370
371 Figure 5. Surface F_{OCS} and F_{CO2} from chamber measurements (brown squares in a-b)
372 from sites 2 and 3. Site 1 was atypical (see section 2.7) and therefore fluxes are not
373 shown. Values for site 1 F_{OCS} and F_{CO2} were -22 ± 0.3 pmolm^{-2}s^{-1} and -83 ± 2 μmolm^{-2}s^{-1}
374 respectively. Error bars indicate standard deviation.

375 3.4. Sensitivity to diffuse light: Mid-day fluxes of OCS and CO_2 were found to be
376 sensitive to changes in the fraction of diffused: total incoming shortwave radiation (*fdiff*;
377 Figure 6b-c). For these analyses, data were separated into three periods corresponding to
378 early summer (DOY 109-180), mid-late summer (DOY 180-240) and early fall (DOY
379 240-297), and binned into three categories: clear sky conditions, partly cloudy, and
380 overcast, defined in sec. 2.7. Mid-day VPD was highest under clear sky conditions and
381 lowest under overcast skies, but was most different across the three periods, during clear
382 skies (Fig. 6a). Consequently, OCS and CO_2 uptake was highest (most negative fluxes)
383 under overcast conditions during the early summer, and generally declined as *fdiff*
384 decreased across all time periods (Fig. 6b-d). Across the three periods, the rate of
385 decrease was much higher as *fdiff* changed from partially cloudy to clear. During the mid-
386 late summer, however, (red diamonds in Fig. 6a-f), the diffuse light effect resulted in
387 GPP and NEE being almost as high as during the early summer. F_{OCS} was also highest
388 under partially cloudy skies during this time, and only showed a very weak decline under
389 completely overcast conditions. Overall, the behavior of OCS and CO_2 fluxes was similar
390 during the later time periods. Leaf relative uptake (LRU; calculated according to eq. 5)
391 was lowest under partly clear skies and highest under overcast conditions. This is because
392 under highly diffuse conditions, carbon uptake is additionally limited by light, whereas
393 F_{OCS} is not (Wehr et al., 2017; Maseyk et al., 2014). The shape of the LRU curves can
394 additionally be explained by examining canopy conductance (Gc; Fig. 6f), which was

11

395 also higher under overcast skies. LRU increased with Gc across all three periods (Fig.
396 6g), and appeared to be constant for Gc greater than ~400 mmolm^{-2}s^{-1}.

397 The diffuse light enhancement of stomatal and canopy conductance is well documented
398 across a range of forest ecosystems (Alton et al., 2007; Cheng et al., 2015; Hollinger et
399 al., 2017; Urban et al., 2007; Wharton et al., 2012). Lower VPD (Fig. 6a) and light levels
400 allow plants to keep stomata open at mid-day and continue fixing CO_2. Lower VPD
401 reduces transpirational losses, and the lack of VPD-induced partial stomatal closure
402 reduces the resistance to CO_2 diffusion into the leaf. Correspondingly, the less directional
403 nature of diffuse solar radiation allows greater penetration into the canopy, thus
404 increasing photosynthesis across the entire canopy, even as a reduction in canopy top leaf
405 photosynthesis is observed due to a reduction in total radiation. In a multi-year analysis at
406 Wind River, Wharton et al., (2012) found that cloudy and partly cloudy sky conditions
407 during the peak-growing season lead to an increase in CO_2 uptake. During our study, Gc
408 was generally higher in the early growing season, but increased as sky conditions
409 changed from clear skies to overcast. This increase was similar across the three time
410 periods, even as the response of OCS and CO_2 fluxes was different across these periods.
411 This indicates that declining soil moisture (Fig. 3b-c) likely limits gas exchange as the
412 summer progresses, even as canopy conductance can be reasonably high under overcast
413 skies.
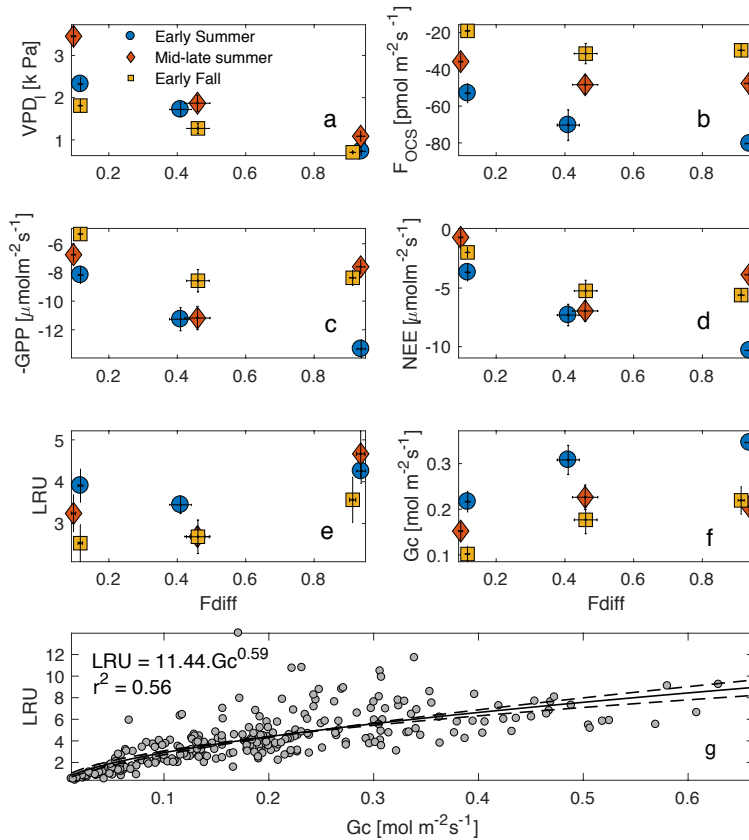
414

415 Figure 6. Mid-day VPD_l, F_{OCS}, NEE and GPP plotted against the fraction of diffuse
416 downwelling shortwave radiation (a-d) for early summer, mid-late summer and early fall

417 of 2015 (these periods are defined in Section 3.4). High values on the x-axis indicate
418 completely overcast or cloudy conditions, whereas as low values indicated clear skies.
419 LRU increases with increasing *fdiff* during each period but the increase is most
420 pronounced in the early summer (e). Gc increases from clear to partly cloudy conditions
421 across the three periods and plateaus during overcast sky conditions (f). Vertical bars
422 indicate 1 standard error. Across the three periods, LRU increased with Gc, and levelled
423 off at Gc values greater than ~ 0.5 mol $m^{-2}s^{-1}$ (g).

424 3.5. Response to heat waves: 2015 was the warmest year in large parts of the Pacific
425 Northwest since records began in the 1930s (Dalton et al., 2017). We observed three
426 distinct heat waves during the 2015 summer. These were in early June (DOY 157-160),
427 end of June- early July (DOY 175-188) and late July-early August (DOY 210-213). The
428 three heat waves are shown as red, yellow and dark purple lines in Fig. 7; the overall time
429 series is shown in blue (mid-day means are plotted for all variables). Mid-day
430 temperatures exceeded 30°C during these heat wave events, while VPD-leaf exceeded 3
431 kPa during the first heat wave and increased to a maximum of 5.3 kPa during the last
432 event (Fig. 7b). During the first event, F_{OCS} was similar to days immediately prior (Fig.
433 7c), but the canopy became a net source of CO_2 during all three events (Fig. 7d). The
434 third events lead to a reduction in F_{OCS}, even though the canopy had received some
435 rainfall in the preceding weeks (Fig. 1c). Water vapor fluxes (Fig. 7e) increased during
436 the first heat wave, compared to days immediately prior. The increased water vapor flux
437 is likely form an increase in transpiration under high VPD_l (red bars in Fig. 7b). Even as
438 canopy conductance (Fig. 7f) is reduced under the third heatwave, high VPD_l ensures a
439 steady transpirational flux (purple bars in Fig. 7e).

13

440
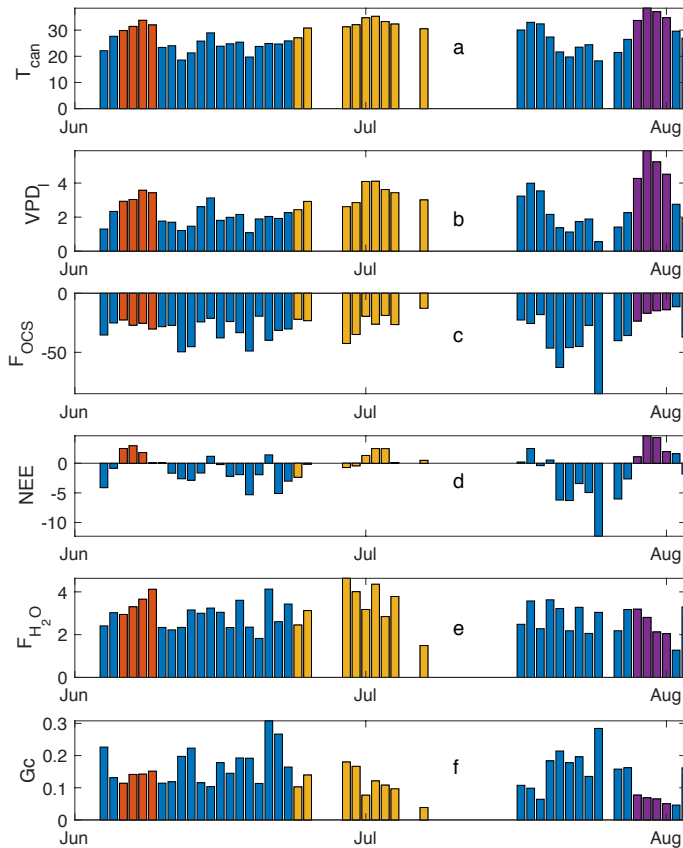
Figure 7. Mid-day means (11am-1pm local time) for three heat wave periods (plotted as red, yellow and purple, while the overall time series is shown in blue). Variables displayed are canopy temperature (°C; a), VPD-leaf (b), F_{OCS} (c), NEE (d), water vapor flux (e), and canopy conductance (Gc, f). Units for each panel are the same as specified in previous figures.

4. Conclusions

Over hourly, daily and seasonal timescales, estimates of F_{OCS} generally tracked fluctuations in GPP, implying stomatal control of carbon, water, and OCS fluxes at the site. We used continuous in-situ measurements of OCS mixing ratios, collocated measurements of water vapor fluxes, and air and canopy temperatures to calculate OCS uptake. We found the forest to be a large sink for OCS, with sink strength peaking during daylight hours. The mean LRU was ~ 4, and varied in response to changing light conditions and canopy conductance. These LRUs are larger than observed from other ecosystem scale studies, but well within the range of reported values (Whelan et al., 2018; Sandoval-Soto et al., 2005). The forest surface was found to be a soil moisture dependent sink of OCS. Ecosystem fluxes of OCS and CO_2 were found to be strongly sensitive to the ratio of diffuse: direct radiation reaching the top of the canopy. Uptake of both OCS and CO_2 increased as sky conditions changed from clear to partly cloudy. A much smaller increase in uptake was observed as sky conditions changed from partly cloudy to overcast, except during the early summer, when soil moisture was not limiting. This change was mediated by the sensitivity of stomata to changing cloudiness and soil

14

462   moisture, as estimated from canopy conductance. Finally, we examined the response of
463   OCS, CO_2 and H_2O fluxes on heatwaves, and found that sequential heatwaves lead to
464   suppression in stomatal gas exchange of all three fluxes.

465   Our results support the growing body of work that suggests ecosystem-scale OCS uptake
466   is controlled by stomatal dynamics. While moist old-growth forests in Pacific
467   Northwestern U.S. do not represent a very large fraction of the global terrestrial surface
468   area, results from this study are likely relevant for other old-growth forests, particularly
469   high LAI and very wet forests with extensive epiphyte cover, which are widespread in the
470   humid tropics.

480   References:

481   Adams, W. W. and Demmig-Adams, B.: Carotenoid composition and down regulation of
482   photosystem II in three conifer species during the winter, Physiol. Plant., 92(3), 451–458,
483   doi:10.1111/j.1399-3054.1994.tb08835.x, 1994.

484   Alton, P. B., North, P. R. and Los, S. O.: The impact of diffuse sunlight on canopy light-
485   use efficiency, gross photosynthetic product and net ecosystem exchange in three forest
486   biomes, Glob. Chang. Biol., 13(4), 776–787, doi:10.1111/j.1365-2486.2007.01316.x,
487   2007.

488   Asaf, D., Rotenberg, E., Tatarinov, F., Dicken, U., Montzka, S. A. and Yakir, D.:
489   Ecosystem photosynthesis inferred from measurements of carbonyl sulphide flux, Nat.
490   Geosci., 6(3), 186–190, doi:10.1038/ngeo1730, 2013.

491   Belviso, S., Reiter, I. M., Loubet, B., Gros, V., Lathière, J., Montagne, D., Delmotte, M.,
492   Ramonet, M., Kalogridis, C., Lebegue, B., Bonnaire, N., Kazan, V., Gauquelin, T.,
493   Fernandez, C. and Genty, B.: A top-down approach of surface carbonyl sulfide exchange
494   by a Mediterranean oak forest ecosystem in Southern France, Atmos. Chem. Phys.
495   Discuss., (June 2012), 1–25, doi:10.5194/acp-2016-525, 2016.

496   Berkelhammer, M., Asaf, D., Still, C., Montzka, S., Noone, D., Gupta, M., Provencal, R.,
497   Chen, H. and Yakir, D.: Constraining surface carbon fluxes using in situ measurements of
498   carbonyl sulfide and carbon dioxide, Global Biogeochem. Cycles, 28(2), 161–179,
499   doi:10.1002/2013GB004644, 2014.

500   Berkelhammer, M., Steen-Larsen, H. C., Cosgrove, A., Peters, A. J., Johnson, R.,
501   Hayden, M. and Montzka, S. A.: Radiation and atmospheric circulation controls on
502   carbonyl sulfide concentrations in themarine boundary layer, J. Geophys. Res., 121(21),
503   13,113-13,128, doi:10.1002/2016JD025437, 2016.

504   Berry, J., Wolf, A., Campbell, J. E., Baker, I., Blake, N., Blake, D., Denning, A. S.,
505   Kawa, S. R., Montzka, S. A., Seibt, U., Stimler, K., Yakir, D. and Zhu, Z.: A coupled
506   model of the global cycles of carbonyl sulfide and CO $_2$: A possible new window on the
507   carbon cycle, J. Geophys. Res. Biogeosciences, 118(2), 842–852,
508   doi:10.1002/jgrg.20068, 2013.

509   Billesbach, D. P., Berry, J. A., Seibt, U., Maseyk, K., Torn, M. S., Fischer, M. L., Abu-
510   Naser, M. and Campbell, J. E.: Growing season eddy covariance measurements of
511   carbonyl sulfide and CO2 fluxes: COS and CO2 relationships in Southern Great Plains
512   winter wheat, Agric. For. Meteorol., 184, 48–55, doi:10.1016/j.agrformet.2013.06.007,
513   2014.

514   Bloem, E., Haneklaus, S., Kesselmeier, J. and Schnug, E.: Sulfur fertilization and fungal
515   infections affect the exchange of H 2S and COS from agricultural crops, J. Agric. Food
516   Chem., 60(31), 7588–7596, doi:10.1021/jf301912h, 2012.

517   Blonquist, J. M., Montzka, S. A., Munger, J. W., Yakir, D., Desai, A. R., Dragoni, D.,
518   Griffis, T. J., Monson, R. K., Scott, R. L. and Bowling, D. R.: The potential of carbonyl
519   sulfide as a proxy for gross primary production at flux tower sites, J. Geophys. Res.
520   Biogeosciences, 116(4), 1–18, doi:10.1029/2011JG001723, 2011.

521   Campbell, J. E., Berry, J., Seibt, U., Smith, S., Nature, S. M.- and 2017, U.: Large
522   historical growth in global terrestrial gross primary production, nature.com, 544(7468),
523   84 [online] Available from: https://www.nature.com/articles/nature22030 (Accessed 29
524   January 2018a), 2017.

525   Campbell, J. E., Whelan, M. E., Berry, J. A., Hilton, T. W., Zumkehr, A., Stinecipher, J.,
526   Lu, Y., Kornfeld, A., Seibt, U., Dawson, T. E., Montzka, S. A., Baker, I. T., Kulkarni, S.,
527   Wang, Y., Herndon, S. C., Zahniser, M. S., Commane, R. and Loik, M. E.: Plant Uptake
528   of Atmospheric Carbonyl Sulfide in Coast Redwood Forests, J. Geophys. Res.
529   Biogeosciences, 122(12), 3391–3404, doi:10.1002/2016JG003703, 2017b.

530   Cheng, S. J., Bohrer, G., Steiner, A. L., Hollinger, D. Y., Suyker, A., Phillips, R. P. and
531   Nadelhoffer, K. J.: Variations in the influence of diffuse light on gross primary
532   productivity in temperate ecosystems, Agric. For. Meteorol., 201, 98–110,
533   doi:10.1016/j.agrformet.2014.11.002, 2015.

534   Commane, R., Meredith, L. K., Baker, I. T., Berry, J. A., Munger, J. W., Montzka, S. A.,
535   Templer, P. H., Juice, S. M., Zahniser, M. S. and Wofsy, S. C.: Seasonal fluxes of
536   carbonyl sulfide in a midlatitude forest, Proc. Natl. Acad. Sci., 112(46), 14162–14167,
537   doi:10.1073/pnas.1504131112, 2015.

538   Dalton, M. M., Dello, K. D., Hawkins, L., Mote, P. W. and Rupp, D. E.: The third

539 Oregon climate assessment report, Oregon Clim. Chang. Res. Institute, Coll. Earth,
540 Ocean Atmos. Sci. Oregon State Univ. Corvallis, OR, 2017.

541 Eastman, P. A. K. and Camm, E. L.: Regulation of photosynthesis in interior spruce
542 during water stress: changes in gas exchange and chlorophyll fluorescence, Tree Physiol.,
543 15(4), 229–235 [online] Available from: http://dx.doi.org/10.1093/treephys/15.4.229,
544 1995.

545 Falk, M., Wharton, S., Schroeder, M., Ustin, S. L. and Paw U, K. T.: Flux partitioning in
546 an old-growth forest: seasonal and interannual dynamics, Tree Physiol., 28(4), 509–520,
547 doi:10.1093/treephys/28.4.509, 2008.

548 Gimeno, T. E., Ogée, J., Royles, J., Gibon, Y., West, J. B., Burlett, R., Jones, S. P.,
549 Sauze, J., Wohl, S., Benard, C., Genty, B. and Wingate, L.: Bryophyte gas-exchange
550 dynamics along varying hydration status reveal a significant carbonyl sulphide (COS)
551 sink in the dark and COS source in the light, New Phytol., 215(3), 965–976,
552 doi:10.1111/nph.14584, 2017.

553 Hilton, T., Whelan, M., Zumkehr, A., … S. K.-N. C. and 2017, U.: Peak growing season
554 gross uptake of carbon in North America is largest in the Midwest USA, nature.com,
555 7(6), 450 [online] Available from: https://www.nature.com/articles/nclimate3272
556 (Accessed 29 January 2018), 2017.

557 Hollinger, A. D. Y., Kelliher, F. M., Byers, J. N., Hunt, J. E., Mcseveny, T. M., Weir, L.,
558 Ecology, S. and Jan, N.: Carbon Dioxide Exchange between an Undisturbed Old-Growth
559 Temperate Forest and the Atmosphere Published by : Wiley Stable URL :
560 http://www.jstor.org/stable/1939390 REFERENCES Linked references are available on
561 JSTOR for this article : You may need to log , , 75(1), 134–150, 2017.

562 Johnson, J. E., Bandy, A. R., Thornton, D. C. and Bates, T. S.: Measurements of
563 atmospheric carbonyl sulfide during the NASA Chemical Instrumentation Test and
564 Evaluation project: Implications for the global COS budget, J. Geophys. Res., 98(D12),
565 23443, doi:10.1029/92JD01911, 1993.

566 Kim, Y., Still, C. J., Hanson, C. V., Kwon, H., Greer, B. T. and Law, B. E.: Canopy skin
567 temperature variations in relation to climate, soil temperature, and carbon flux at a
568 ponderosa pine forest in central Oregon, Agric. For. Meteorol., 226–227, 161–173,
569 doi:10.1016/j.agrformet.2016.06.001, 2016.

570 Kitz, F., Gerdel, K., Hammerle, A., Laterza, T., Spielmann, F. M. and Wohlfahrt, G.: In
571 situ soil COS exchange of a temperate mountain grassland under simulated drought,
572 Oecologia, 183(3), 851–860, doi:10.1007/s00442-016-3805-0, 2017.

573 Kooijmans, L. M. J. J., Maseyk, K., Seibt, U., Sun, W., Vesala, T., Mammarella, I.,
574 Kolari, P., Aalto, J., Franchin, A., Vecchi, R., Valli, G. and Chen, H.: Canopy uptake
575 dominates nighttime carbonyl sulfide fluxes in a boreal forest, Atmos. Chem. Phys.,
576 17(18), 11453–11465, doi:10.5194/acp-17-11453-2017, 2017.

577   Launois, T., Peylin, P., Belviso, S. and Poulter, B.: A new model of the global
578   biogeochemical cycle of carbonyl sulfide - Part 2: Use of carbonyl sulfide to constrain
579   gross primary productivity in current vegetation models, Atmos. Chem. Phys., 15(16),
580   9285–9312, doi:10.5194/acp-15-9285-2015, 2015.

581   Maseyk, K., Berry, J. A., Billesbach, D., Campbell, J. E., Torn, M. S., Zahniser, M. and
582   Seibt, U.: Sources and sinks of carbonyl sulfide in an agricultural field in the Southern
583   Great Plains, Proc. Natl. Acad. Sci., 111(25), 9064–9069, doi:10.1073/pnas.1319132111,
584   2014.

585   Notholt, J., Kuang, Z., Rinsland, C. P., Toon, G. C., Rex, M., Jones, N., Albrecht, T.,
586   Deckelmann, H., Krieg, J. and Weinzierl, C.: Enhanced upper tropical tropospheric COS:
587   Impact on the stratospheric aerosol layer, Science (80-.)., 300(5617), 307–310, 2003.

588   Parker, G. G., Harmon, M. E., Lefsky, M. A., Chen, J., Pelt, R. Van, Weis, S. B.,
589   Thomas, S. C., Winner, W. E., Shaw, D. C. and Frankling, J. F.: Three-dimensional
590   Structure of an Old-growth Pseudotsuga-Tsuga Canopy and Its Implications for Radiation
591   Balance, Microclimate, and Gas Exchange, Ecosystems, 7(5), 440–453,
592   doi:10.1007/s10021-004-0136-5, 2004.

593   Paw U, K. T., Falk, M., Suchanek, T. H., Ustin, S. L., Chen, J., Park, Y.-S., Winner, W.
594   E., Thomas, S. C., Hsiao, T. C., Shaw, R. H., King, T. S., Pyles, R. D., Schroeder, M. and
595   Matista, A. A.: Carbon Dioxide Exchange between an Old-Growth Forest and the
596   Atmosphere, Ecosystems, 7(5), 513–524, doi:10.1007/s10021-004-0141-8, 2004.

597   Protoschill-Krebs, G Wilhelm, C Kesselmeier, J.: Consumption of carbonyl sulphide
598   (COS) by higher plant carbonic anhydrase (CA), Atmos. Environ., 30(18), 3151–3156
599   [online] Available from:
600   https://www.sciencedirect.com/science/article/pii/135223109600026X (Accessed 29
601   January 2018), 1996.

602   Protoschill-Krebs, G. and Kesselmeier, J.: Enzymatic pathways for the consumption of
603   carbonyl sulphide (COS) by higher plants, Bot. Acta, 105, 206–212 [online] Available
604   from: http://onlinelibrary.wiley.com/doi/10.1111/j.1438-8677.1992.tb00288.x/full
605   (Accessed 29 January 2018), 1992.

606   Reichstein, M., Falge, E., Baldocchi, D., Papale, D., Aubinet, M., Berbigier, P.,
607   Bernhofer, C., Buchmann, N., Gilmanov, T. and Granier, A.: On the separation of net
608   ecosystem exchange into assimilation and ecosystem respiration: review and improved
609   algorithm, Glob. Chang. Biol., 11(9), 1424–1439, 2005.

610   Sandoval-Soto, L., Stanimirov, M., von Hobe, M., Schmitt, V., Valdes, J., Wild, A. and
611   Kesselmeier, J.: Global uptake of carbonyl sulfide (COS) by terrestrial vegetation:
612   Estimates corrected by deposition velocities normalized to the uptake of carbon dioxide
613   (CO_2), Biogeosciences Discuss., 2(1), 183–201,
614   doi:10.5194/bgd-2-183-2005, 2005.

615   Seibt, U., Kesselmeier, J., Sandoval-Soto, L., Kuhn, U. and Berry, J. A.: A kinetic

616   analysis of leaf uptake of COS and its relation to transpiration, photosynthesis and carbon
617   isotope fractionation, Biogeosciences, 7(1), 333–341, doi:10.5194/bg-7-333-2010, 2010.

618   Shaw, D., Franklin, J., Bible, K., Klopatek, J., Freeman, E., Greene, S. and Parker, G.:
619   Ecological Setting of the Wind River Old-growth Forest, Ecosystems, 7(5), 427–439,
620   doi:10.1007/s10021-004-0135-6, 2004.

621   Stimler, K., Nelson, D. and Yakir, D.: High precision measurements of atmospheric
622   concentrations and plant exchange rates of carbonyl sulfide using mid-IR quantum
623   cascade laser, Glob. Chang. Biol., 16(9), 2496–2503, doi:10.1111/j.1365-
624   2486.2009.02088.x, 2010a.

625   Stimler, K., Montzka, S. A., Berry, J. A., Rudich, Y. and Yakir, D.: Relationships
626   between carbonyl sulfide (COS) and CO2 during leaf gas exchange, New Phytol., 186(4),
627   869–878, doi:10.1111/j.1469-8137.2010.03218.x, 2010b.

628   Sun, W., Maseyk, K., Lett, C. and Seibt, U.: Litter dominates surface fluxes of carbonyl
629   sulfide in a Californian oak woodland, J. Geophys. Res. G Biogeosciences, 121(2), 438–
630   450, doi:10.1002/2015JG003149, 2016.

631   Urban, O., Janouš, D., Acosta, M., Czerný, R., Marková, I., Navrátil, M., Pavelka, M.,
632   Pokorný, R., Šprtová, M., Zhang, R., Špunda, V. R., Grace, J. and Marek, M. V.:
633   Ecophysiological controls over the net ecosystem exchange of mountain spruce stand.
634   Comparison of the response in direct vs. diffuse solar radiation, Glob. Chang. Biol.,
635   13(1), 157–168, doi:10.1111/j.1365-2486.2006.01265.x, 2007.

636   Wehr, R., Commane, R., Munger, J. W., Barry Mcmanus, J., Nelson, D. D., Zahniser, M.
637   S., Saleska, S. R. and Wofsy, S. C.: Dynamics of canopy stomatal conductance,
638   transpiration, and evaporation in a temperate deciduous forest, validated by carbonyl
639   sulfide uptake, Biogeosciences, 14(2), 389–401, doi:10.5194/bg-14-389-2017, 2017.

640   Wharton, S. and Falk, M.: Climate indices strongly influence old-growth forest carbon
641   exchange, Environ. Res. Lett., 11(4), 1–11, doi:10.1088/1748-9326/11/4/044016, 2016.

642   Wharton, S., Falk, M., Bible, K., Schroeder, M. and Paw U, K. T.: Old-growth CO 2 flux
643   measurements reveal high sensitivity to climate anomalies across seasonal, annual and
644   decadal time scales, Agric. For. Meteorol., 161, 1–14,
645   doi:10.1016/j.agrformet.2012.03.007, 2012.

646   Whelan, M. E., Hilton, T. W., Berry, J. A., Berkelhammer, M., Desai, A. R. and
647   Campbell, J. E.: Carbonyl sulfide exchange in soils for better estimates of ecosystem
648   carbon uptake, Atmos. Chem. Phys., 16(6), 3711–3726, 2016.

649   Whelan, M. E., Lennartz, S. T., Gimeno, T. E., Wehr, R., Wohlfahrt, G., Wang, Y.,
650   Kooijmans, L. M. J., Hilton, T. W., Belviso, S., Peylin, P., Commane, R., Sun, W., Chen,
651   H., Kuai, L., Mammarella, I., Maseyk, K., Berkelhammer, M., Li, K.-F., Yakir, D.,
652   Zumkehr, A., Katayama, Y., Ogée, J., Spielmann, F. M., Kitz, F., Rastogi, B.,
653   Kesselmeier, J., Marshall, J., Erkkilä, K.-M., Wingate, L., Meredith, L. K., He, W., Bunk,

654   R., Launois, T., Vesala, T., Schmidt, J. A., Fichot, C. G., Seibt, U., Saleska, S., Saltzman,
655   E. S., Montzka, S. A., Berry, J. A. and Campbell, J. E.: Reviews and Syntheses: Carbonyl
656   Sulfide as a Multi-scale Tracer for Carbon and Water Cycles, Biogeosciences Discuss.,
657   (October), 1–97, doi:10.5194/bg-2017-427, 2017.

658   Winner, W., Thomas, S., Berry, J., Bond, B., Cooper, C., Hinckley, T., Ehleringer, J.,
659   Fessenden, J., Lamb, B., McCarthy, S., McDowell, N., Phillips, N. and Williams, M.:
660   Canopy Carbon Gain and Water Use: Analysis of Old-growth Conifers in the Pacific
661   Northwest, Ecosystems, 7(5), 482–497, doi:10.1007/s10021-004-0139-2, 2004.

662   Wohlfahrt, G., Brilli, F., Hörtnagl, L., Xu, X., Bingemer, H., Hansel, A. and Loreto, F.:
663   Carbonyl sulfide (COS) as a tracer for canopy photosynthesis, transpiration and stomatal
664   conductance: Potential and limitations, Plant, Cell Environ., 35(4), 657–667,
665   doi:10.1111/j.1365-3040.2011.02451.x, 2012.

666   Woodruff, D. R., Mcculloh, K. A., Warren, J. M., Meinzer, F. C. and Lachenbruch, B.:
667   Impacts of tree height on leaf hydraulic architecture and stomatal control in Douglas-fir,
668   Plant, Cell Environ., 30(5), 559–569, doi:10.1111/j.1365-3040.2007.01652.x, 2007.

669